JACS
JOURNAL OF THE AMERICAN CHEMICAL SOCIETY
Article
Cite This: J. Am. Chem. Soc. XXXX, XXX, XXX−XXX
pubs.acs.org/JACS

Determination of Energy-Level Alignment in Molecular Tunnel Junctions by Transport and Spectroscopy: Self-Consistency for the Case of Oligophenylene Thiols and Dithiols on Ag, Au, and Pt Electrodes

Zuoti Xie,[†] Ioan Bâldea,[*,‡] and C. Daniel Frisbie[*,†]

[†]Department of Chemical Engineering and Materials Science, University of Minnesota, Minneapolis, Minnesota 55455, United States

[‡]Theoretische Chemie, Universität Heidelberg, INF 229, D-69120 Heidelberg, Germany

Supporting Information

ABSTRACT: We report detailed measurements of transport and electronic properties of molecular tunnel junctions based on self-assembled monolayers (SAMs) of oligophenylene monothiols (OPT*n*, *n* = 1−3) and dithiols (OPD*n*, *n* = 1−3) on Ag, Au, and Pt electrodes. The junctions were fabricated with the conducting probe atomic force microscope (CP-AFM) platform. Fitting of the current−voltage (*I*−*V*) characteristics for OPT*n* and OPD*n* junctions to the analytical single-level tunneling model allows extraction of both the HOMO-to-Fermi-level offset (ε_h) and the average molecule−electrode coupling (Γ) as a function of molecular length (*n*) and electrode work function (Φ). Significantly, direct measurements of ε_h^{UPS} by ultraviolet photoelectron spectroscopy (UPS) for OPT*n* and OPD*n* SAMs on Ag, Au, and Pt agree remarkably well with the transport estimates ε_h^{trans}, providing strong support—beyond the high quality *I*−*V* simulations—for the relevance of the analytical single-level model to simple molecular tunnel junctions. Because the UPS measurements involve SAMs bonded to only one metal contact, the correspondence of ε_h^{UPS} and ε_h^{trans} also indicates that the top contact has a weak effect on the HOMO energy. Corroborating ab initio calculations definitively rule out a dominant contribution of image charge effects to the magnitude of ε_h. Thus, the effective molecular tunnel barrier ε_h is determined, and essentially pinned, by the formation of a single metal−S covalent bond per OPT*n* or OPD*n* molecule.

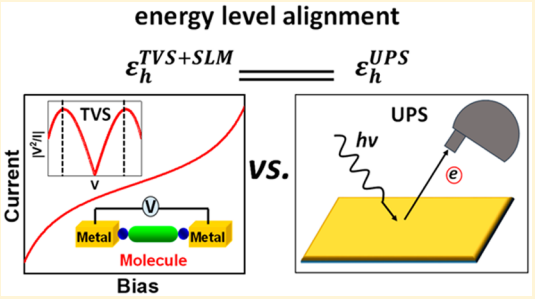

INTRODUCTION

Relating charge-transport properties to the electronic structure of metal−molecule−metal junctions is an important fundamental goal for the field of molecular electronics that is essential to the rational design of junctions with prescribed current−voltage (*I*−*V*) behavior.[1−22] Generally speaking, the approach taken by many research groups is to compare conductance measurements (typically not full *I*−*V* behavior) with the predictions of density functional theory (DFT) calculations.[23−30] In this case, DFT is employed (1) to estimate the electronic structure of the junction,[23−30] e.g., the offset (ε_h or ε_l) of the HOMO or LUMO from the junction Fermi level, and the molecule-electrode coupling (Γ), Figure 1A and (2) to compute the electron or hole transmission function as a function of applied bias.[25−34] The correspondence of the calculation with the experimental conductance measurements (usually over a limited voltage window, perhaps even just at a single voltage) is employed to establish the charge transport-electronic structure relationship.

It is of course desirable to have an independent experimental measurement of electronic structure inside a nanoscale metal−molecule−metal junction that can be compared to quantum chemical calculations. Molecular junctions employing a gate electrode enable transport spectroscopy that indeed provides transport and electronic structure information simultaneously on single molecules or molecular ensembles, facilitating comparisons to computational predictions.[5,35−40] This elegant approach to the transport-electronic structure problem is not available for two-terminal molecular junctions. It is desirable to address this issue, namely to find a way to extract electronic structure information directly from two terminal transport measurements and to compare the results with an independent spectroscopic measurement. This provides a consistency check and substantiation (or required revision) of the proposed transport−electronic structure relationship. Accomplishing this for simple two terminal molecular junctions is the goal of this report.

Recent work by the authors, independently[41] and collaboratively,[42−47] has shown that the compact, analytical single-level model (SLM), derived from the Landauer picture and subject to certain approximations, can be employed

Received: December 14, 2018
Published: January 28, 2019

DOI: 10.1021/jacs.8b13370
J. Am. Chem. Soc. XXXX, XXX, XXX−XXX

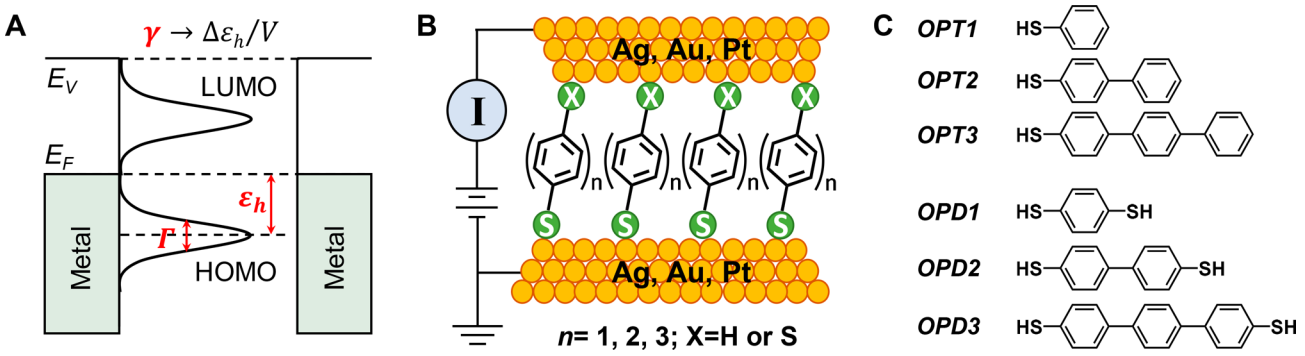

Figure 1. (A) Typical molecular junction electronic structure with key parameters ε_h, Γ, and γ. (B) Schematic representation of the CP-AFM junction. A metal-coated AFM tip is brought into contact with a SAM of OPT*n* or OPD*n* on Ag, Au, or Pt substrates. (C) Molecular structures of OPT*1*−*3* and OPD*1*−*3*.

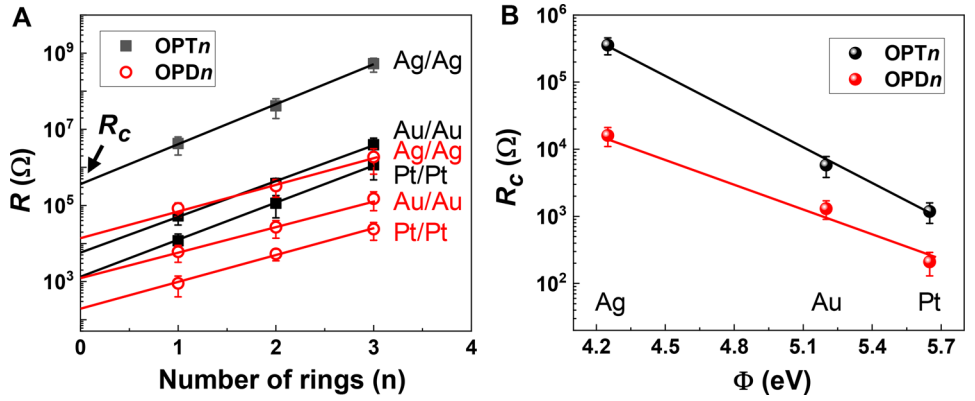

Figure 2. (A) Semilog plot of low-bias resistance for OPT*n* and OPD*n* *versus* number of phenyl rings (n = 1−3). (B) Contact resistance (R_c) for OPT*n* and OPD*n* *versus* the work functions of the electrodes. The work function of the bare Ag, Au, and Pt electrodes are 4.25 eV, 5.2 eV and 5.65 eV, respectively.

productively to extract the HOMO (or LUMO) position ε_h^{trans} (or ε_l^{trans}) and the molecule−electrode coupling Γ from junction I−V characteristics. Validation for the SLM has so far included (1) its ability to fit the I−V characteristics for a wide variety of simple molecular junctions extremely well with physically reasonable values for ε_h^{trans} and Γ and (2) its prediction of a universal master curve that precisely matches the I−V characteristics of molecular junctions consisting of aliphatic and aromatic molecules with conductances varying over 5 orders of magnitude.[45,48] In this paper, we employ the SLM to extract ε_h^{trans} and Γ for junctions based on self-assembled monolayers (SAMs) of two series of molecules, oligophenylene monothiols (OPT*n*, n = 1,2,3) and dithiols (OPD*n*, n = 1−3), on Ag, Au, and Pt electrodes, Figure 1. We then compare ε_h^{trans} obtained from the transport analysis of the 18 different junctions to 18 values of ε_h^{UPS} measured independently by ultraviolet photoelectron spectroscopy (UPS) for SAMs of OPT*n* and OPD*n* on Ag, Au, and Pt. To our knowledge, there are few reports that correlate electronic spectroscopy of SAMs with molecular junction transport measurements,[49−54] and so far none in which a principal property, namely ε_h, obtained from both transport and spectroscopy is compared for consistency. We find remarkably good agreement between transport- and UPS-derived ε_h for the cases of OPT*n* and OPD*n*, which is perhaps surprising in that clearly the transport measurement involves two contacts to each SAM, while the UPS analysis occurs on "half the junction", namely just the SAM on the metal substrate; there is no top contact. The close agreement of the two measurements of ε_h for 18 different types of junctions has a number of important consequences: it provides important insight into the band lineup problem for OPT*n* and OPD*n* with one contact vs two, it supports the physical picture of transport in these systems suggested by Figure 1A, and it confirms the SLM as a valuable theoretical tool for analysis of I−V characteristics of simple molecular junctions. We note for transparency that the I−V characteristics and SLM analysis of the OPD*n* system were reported in an earlier publication,[42] and those results are reproduced here for the purpose of comparison to the OPT*n* system (i.e., for the comparison of the role of one chemical contact versus two). Importantly, UPS analysis and a comparison of ε_h^{trans} versus ε_h^{UPS} for OPD*n* were not reported previously and constitute a new and important aspect of the current study.

While the correspondence of ε_h derived from transport and spectroscopic measurements is our main result, we conclude this report with a discussion of the implications of the measured ε_h on the mechanisms of energy level lineup in molecular junctions, specifically the roles of image charge effects versus metal−molecule chemical bonding on the magnitude of ε_h.

EXPERIMENTAL METHODS

Materials. Gold nuggets (99.999% pure) were purchased from Mowrey, Inc. (St. Paul, MN). Silver pellets (99.99% pure) were purchased from Kurt J. Lesker Co.. Evaporation boats and chromium evaporation rods were purchased from R. D. Mathis (Long Beach,

DOI: 10.1021/jacs.8b13370
J. Am. Chem. Soc. XXXX, XXX, XXX−XXX

CA). Platinum and titanium for e-beam evaporation were purchased from Kamis, Inc. (Mahopac Falls, NY). Silicon (100) wafers were obtained from WaferNet (San Jose, CA). Contact mode AFM tips (DNP silicon nitride probes) were purchased from Bruker AFM Probes. The benzene-1,4-dithiol (OPD1) 99%, *p*-terphenyl-4,4″-dithiol (OPD3) 96%, thiophenol (OPT1) 97%, biphenyl-4-thiol (OPT2) 97%, and 1,1′,4′,1″-terphenyl-4-thiol (OPT3) 97% used in this study were purchased from Sigma-Aldrich, and biphenyl-4,4′-dithiol(OPD2) 95% was purchased from TCI America.

Monolayer Growth and Characterization. Preparation of conducting tips and template-stripped flat Ag, Au, and Pt substrates are described in a previous publication.[42] SAMs were formed by immersing clean template-stripped flat metal substrates into ethanol solutions of the molecules at a concentration of ∼1 mM for 20 h. The chemical composition and thickness of the OPT and OPD SAMs' were characterized by XPS (Figures S1 and S2 and Table S1 in the Supporting Information). Previously, we have characterized OPT and OPD SAMs by spectroscopic ellipsometry, Rutherford backscattering spectrometry, and nuclear reaction analysis.[42,55,56] The HOMO−Fermi level offset of OPT and OPD SAMs on metals was measured by UPS (Figure S3 in the Supporting Information). During UPS acquisition, −5 V was applied to the sample to obtain the secondary electron cutoff to calculate the work function of the samples (cf. Figure S6 in the Supporting Information). Details of the XPS and UPS measurements are described in the Supporting Information. Scanning Kelvin probe microscopy (SKPM) measurements were used to determine the work function (Φ) with and without a SAM adsorbed on the metal surface ($\Phi_{SAM} = \Phi + \Delta\Phi$) (see Table 2). SKPM measurements were carried out using the same instrument that was employed for *I*−*V* characterization. The AFM instrument was housed in an Ar-filled glovebox (H_2O, O_2 < 0.1 ppm). The work functions of the samples were referenced to the UPS value of benzene-1,4-dithiol on an Au substrate.

Transport Measurements. Current−voltage measurements were completed by mounting the substrates in the AFM and bringing the metal-coated tip into contact with the SAM under ∼1 nN of the applied compressive load (Figure 1B). Voltages were applied to the tip with a Keithley model 236 source-measure unit operated in "DC mode". Voltage was swept at the tip, the sample was grounded, and current−voltage characteristics were recorded ($V > 0$ means positive voltage on the tip). All measured *I*−*V* curves crossed over from practically linear at low biases to gradually more nonlinear at higher biases. The inverse of the slope of the linear portion of the *I*−*V* characteristic was used to define a junction (low bias) resistance R. The tunneling attenuation parameter β and contact resistance R_c were extracted with high certainty from plots of the low bias resistance versus molecular length. Voltage sweeps to ±1.2−1.5 V were applied to observe the pronounced nonlinear (*I*−*V*) behavior.

RESULTS AND DISCUSSION

At the outset, we reiterate the point made in the Introduction that the charge-transport properties of OPD*n* junctions with Ag, Au, and Pt contacts have been reported previously.[42] The key extracted parameters ε_h and Γ are included here with the new monothiol OPT*n* data for the purpose of direct comparison. In addition, we present previously unreported UPS data for both OPT*n* and OPD*n* systems. A comparison of the transport and spectroscopy data sets for OPT*n* and OPD*n* allows us to make important conclusions about the role of chemical versus physical contacts on the energy level lineup problem for these π-conjugated systems.

Low Bias Resistance. In the case of off-resonant tunneling, it is known that low bias resistance scales exponentially with molecular length[2]

$$R_n = R_c \exp(\beta n L_0) \quad (1)$$

where R_c is the effective contact resistance, β is the tunneling decay parameter, L_0 is the molecular length in repeat units, and n is the number of repeat units. From the slope of a semilog plot of $R = R_n$ versus the number of units in the chain n, one can determine the tunneling attenuation factor β, and its intercept at $n = 0$ gives the effective contact resistance R_c. The low bias resistances of the junctions were calculated from the average of approximately 100−150 *I*−*V* traces within ±0.1 V (Table 1). The linear relationships for OPT*n* and OPD*n* in Figure 2 indicate that the data fit well within the off-resonance tunneling model described by eq 1. The β values of OPT*n* and OPD*n* found here are independent of metal work functions within the experimental uncertainty but strongly dependent on the number of the linkers, as reported previously for other SAM systems.[42,51,57,58] The measured β-values are 2.3 and 1.5 per phenyl ring, or 0.54 and 0.37 Å^{-1}, for the OPT*n* and OPD*n* wires, respectively. The contact resistances R_c, given by the intercepts of the Figure 2A plots, change markedly by altering the type of the metals, Figure 2B, as is now well-known.[57] For the electrodes studied (Ag, Au, and Pt), Φ increases by 1.4 eV and R_c decreases by a factor of 300 and 70 for OPT*n* and OPD*n*, respectively. The decreases in both R and R_c with Φ in Figure 2 indicate hole-type (HOMO-mediated tunneling), i.e., higher work function brings the metallic Fermi level closer to the HOMO.

Table 1. Summary of the Main Results for OPT*n* CP-AFM Junctions: β Value in Å^{-1}, Contact Resistance R_c, and Low Bias Resistance of the Junctions (Ω) and Transition Voltages $V_{t\pm}$ (V)[a]

electrode	quantity	OPT1	OPT2	OPT3
Ag/Ag	R	4.22×10^6	4.12×10^7	5.27×10^8
β = 0.58 Å^{-1}	V_{t+}	1.18	0.96	0.79
$R_c = 3.55 \times 10^5$	$\lvert V_{t-}\rvert$	1.31	1.1	0.94
Au/Au	R	5.28×10^4	3.78×10^5	1.93×10^6
β = 0.51 Å^{-1}	V_{t+}	0.94	0.81	0.67
$R_c = 5.79 \times 10^3$	$\lvert V_{t-}\rvert$	1.08	0.98	0.87
Pt/Pt	R	1.18×10^4	1.14×10^5	1.17×10^6
β = 0.55 Å^{-1}	V_{t+}	0.83	0.72	0.6
$R_c = 1.18 \times 10^3$	$\lvert V_{t-}\rvert$	0.97	0.84	0.69

[a]The corresponding data for OPD*n* are found in ref 42.

Analysis of *I*−*V* Traces. For a more comprehensive examination of transport properties, we investigated the nonlinear (higher bias) regime of the *I*−*V* characteristics. Parts A and B of Figure 3 show the representative linear and semilog plots of the average *I*−*V* curves over ±1.3 V for the Au−OPT*n*−Au junctions. Each average *I*−*V* trace is nearly, but not perfectly, symmetric with respect to zero bias; slightly higher current is observed for positive tip bias. For a given voltage, the current decreases exponentially with length. As shown in Figure 3C, we analyze the shape of these curves by recasting the plots on new axes, $|V^2/I|$ vs V.[48,59] This type of plot gives a peak maximum, which corresponds to the point where the differential conductance is two times larger than the nominal pseudo-ohmic conductance.[42,48] This approach is an alternative version of transition voltage spectroscopy (TVS), and the voltage at peak maximum and the transition voltage V_t (originally defined as the bias at the minimum of the Fowler-Nordheim plot[60]) are mathematically identical.[48,59]

Table 1 lists the V_t values at negative and positive bias for 9 OPT*n* junctions. In contrast to the independence of bias

DOI: 10.1021/jacs.8b13370
J. Am. Chem. Soc. XXXX, XXX, XXX−XXX

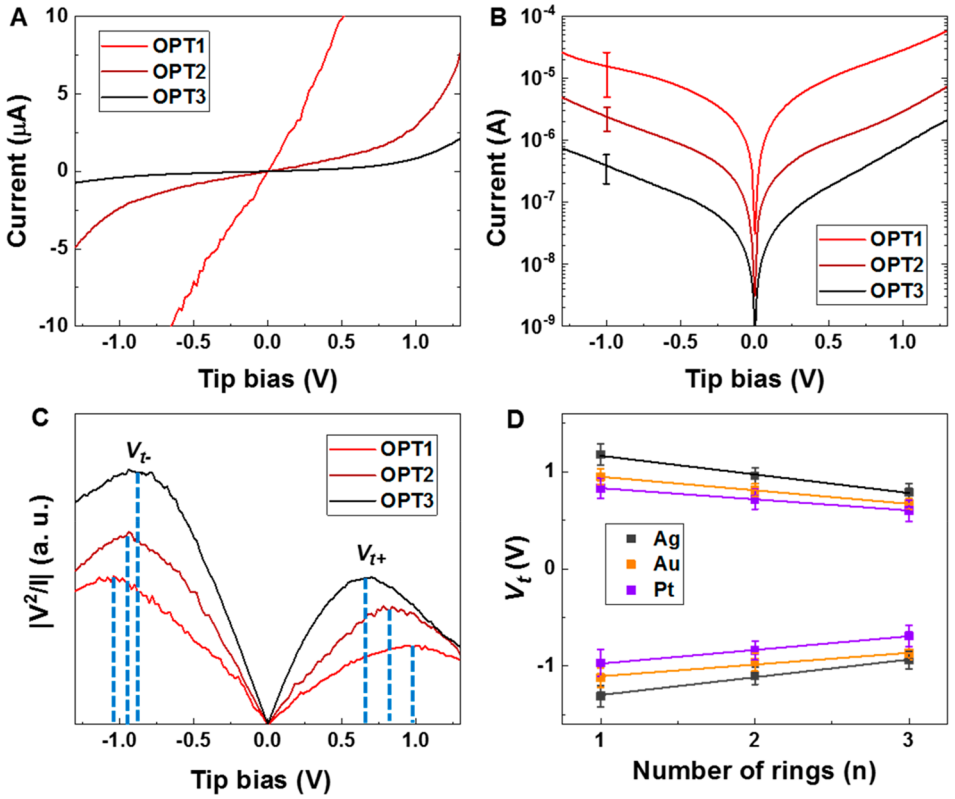

Figure 3. (A) Representative linear and (B) semilog plots of average I–V curves and (C) transition voltage spectra of Au–OPTn–Au junctions. Transition voltages (V_t) are the voltages at the peak maxima, as shown. (D) Transition voltages of Ag–OPTn–Ag, Au–OPTn–Au, and Pt–OPTn–Pt junctions.

Table 2. Key Electronic Structure Parameters Including the Energy offset ε_h^{trans}, Conductance of Junctions G, Average Coupling Γ, and Orbital Voltage Shift Coefficient γ for OPTn and OPDn via the Single-Level Model (Transport)[a]

metal	quantity	OPT1	OPT2	OPT3	OPD1	OPD2	OPD3
Ag	ε_h^{trans}	1.08	0.89	0.74	1.00	0.87	0.73
	ε_h^{UPS}	1.12	0.99	0.92	0.83	0.80	0.79
	G	2.34×10^{-7}	2.43×10^{-8}	1.90×10^{-9}	1.20×10^{-5}	3.09×10^{-6}	5.34×10^{-7}
	Γ	7.14	1.88	0.44	43.94	19.45	6.82
	γ	0.023	0.029	0.038	0	0.004	−0.005
	Φ_{SAM}^{UPS}	3.84	3.96	4.03	4.84	4.93	4.89
	Φ_{SAM}^{SKPM}	4	4.14	4.12	4.61	4.55	4.55
Au	ε_h^{trans}	0.87	0.76	0.66	0.87	0.73	0.56
	ε_h^{UPS}	0.77	0.72	0.68	0.82	0.74	0.68
	G	1.89×10^{-5}	2.65×10^{-6}	5.18×10^{-7}	1.65×10^{-4}	3.73×10^{-5}	6.65×10^{-6}
	Γ	52.65	16.82	4.52	141.65	56.57	18.34
	γ	0.036	0.037	0.055	0.004	−0.005	−0.003
	Φ_{SAM}^{UPS}	4.72	4.24	4.11	4.72	4.72	4.8
	Φ_{SAM}^{SKPM}	4.78	4.36	4.27	4.72	4.77	4.72
Pt	ε_h^{trans}	0.77	0.67	0.56	0.75	0.63	0.49
	ε_h^{UPS}	0.78	0.69	0.62	0.81	0.72	0.60
	G	8.47×10^{-5}	8.77×10^{-6}	8.55×10^{-7}	1.11×10^{-3}	1.88×10^{-4}	4.17×10^{-5}
	Γ	96.30	27.00	6.98	317.63	109.79	40.14
	γ	0.034	0.033	0.030	−0.005	0	−0.012
	Φ_{SAM}^{UPS}	4.52	4.48	4.37	4.81	4.84	4.77
	Φ_{SAM}^{SKPM}	4.24	4.27	4.27	4.45	4.59	4.66

[a]Also included are ε_h^{UPS} and work function for OPTn and OPDn by UPS (Φ_{SAM}^{UPS}) and by SKPM (Φ_{SAM}^{SKPM}). Units: ε_h in eV, G in S, Γ in meV obtained from eq 6 by assuming N = 70 molecules for OPTn and N = 80 molecules for OPDn according to the Maugis–Dugdale (MD) model of contact mechanics, Φ in eV.[46,55] Details of the work function determination are described in the Supporting Information (cf. Figure S6). The UPS data have an error of ±0.1 eV.

polarity for V_t in OPDn symmetric junctions ($|V_{t-}| = V_{t+}$),[42] the V_t of OPTn junctions show bias polarity dependence $|V_{t-}| > V_{t+}$. Also, V_t decreases with increasing length of OPTn, and it also decreases with increasing work function of the contact

DOI: 10.1021/jacs.8b13370
J. Am. Chem. Soc. XXXX, XXX, XXX–XXX

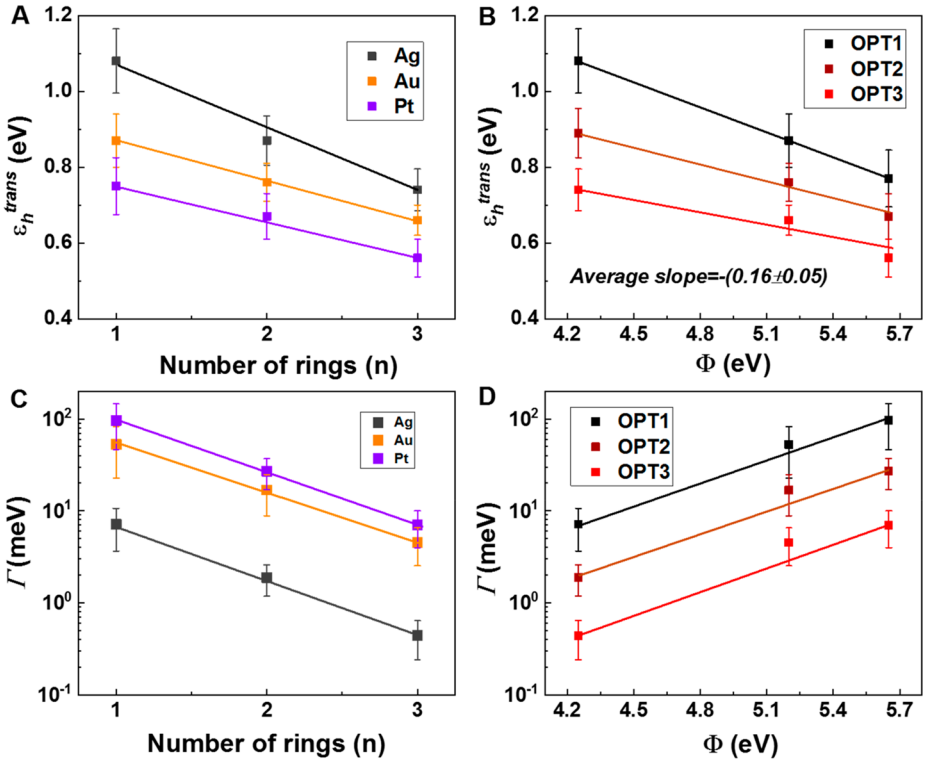

Figure 4. HOMO offset (or effective tunneling barrier) ε_h^{trans} for metal−OPTn−metal junctions as a function of (A) molecular length n and (B) bare electrode work function Φ. The average molecule−electrode coupling (or average level width) Γ of metal−OPTn−metal junctions as a function of (C) molecular length n and (D) bare electrode work function Φ (metal = Ag, Au, Pt; n = 1, 2, 3).

metals, as shown in Figure 3D. Importantly, V_t can be employed to calculate the effective energy offset ε_h of the junctions by using the SLM.[41,42] In the case of molecular junctions with asymmetric $I-V$ characteristics ($|V_{t-}| \neq V_{t+}$, e.g., OPTn), the magnitude of the energy offset of the occupied level ($\varepsilon_h = E_F - E_{HOMO} > 0$) that dominates the charge transport is expressed as follows:[41]

$$\varepsilon_h = 2\frac{e|V_{t+}V_{t-}|}{\sqrt{V_{t+}^2 + 10|V_{t+}V_{t-}|/3 + V_{t-}^2}} \quad (2)$$

For *symmetric* junctions ($V_{t-} \approx V_{t+}$), the correlation between transition voltage V_t and the effective tunneling barrier ε_h is $\varepsilon_h = \sqrt{3}V_t/2e$.[41,42] For *asymmetric* junctions, the molecular orbital (HOMO in this case) energy $E_{HOMO}(V)$ in a biased junction ($V \neq 0$) is shifted with respect to its position in the absence of bias $E_{HOMO} \equiv E_{HOMO}(V = 0)$ by a quantity proportional to V[41,61]

$$E_{HOMO}(V) = E_{HOMO} + \gamma eV,$$
$$\varepsilon_h(V) = E_F - E_{HOMO}(V) = \varepsilon_h - \gamma eV \quad (3)$$

where the orbital shift coefficient γ is given by

$$\gamma = -\frac{1}{2}\frac{V_{t+} + V_{t-}}{\sqrt{V_{t+}^2 + 10|V_{t+}V_{t-}|/3 + V_{t-}^2}} \quad (4)$$

The $I-V$ characteristics are then given as[41,42]

$$I = GV\frac{\varepsilon_h^2}{[\varepsilon_h(V)]^2 - (eV/2)^2} = GV\frac{\varepsilon_h^2}{(\varepsilon_h + \gamma eV)^2 - (eV/2)^2} \quad (5)$$

The zero-bias conductance $G = 1/R$ of the CP-AFM junction can be expressed as follows

$$G = NG_0\frac{\Gamma^2}{\varepsilon_h^2} \quad (6)$$

where $\Gamma = \sqrt{\Gamma_s\Gamma_t} = \varepsilon_h\sqrt{G/(NG_0)}$ is the average molecule-electrode coupling, Γ_s and Γ_t are determined by the molecular coupling to the substrate (s) and tip (t), respectively ($\Gamma_s \approx \Gamma_t$ in symmetric junctions), $G_0 = 2e^2/h$ is the quantum conductance, and N is the number of molecules participating in the transport.

The effective energy offsets ε_h^{trans} for OPTn molecular junctions determined via eq 2 are listed in Table 2 and are plotted in Figure 4. The trend in ε_h^{trans} with molecular length for Ag, Au, and Pt contacts is shown in Figure 4A, where it is clear that ε_h^{trans} decreases systematically with n, similar to our previous report for OPDn.[42] The dependence of ε_h^{trans} on the bare electrode work function Φ is evident in Figure 4B. The fact that the slopes are significantly less than one is an indication of Fermi level pinning,[42−44,51] i.e., large changes in contact work function (~1.4 eV) produce only relatively modest changes (~0.2 eV) in ε_h^{trans}, as has also been reported before for several different molecular junctions.[42−44,51] Notably, the relatively weak dependence of the effective tunneling barrier ε_h^{trans} on molecular length n and metal work function Φ evident in Figure 4A,B cannot be responsible for the much larger (orders of magnitude) differences in resistance with n and Φ shown in Figure 2. It is the molecule−electrode couplings Γ, calculated by eq 6, that drastically change with n and Φ, Table 2 and Figure 4C,D. The strength of the molecule−electrode couplings of OPT junctions decreases

DOI: 10.1021/jacs.8b13370
J. Am. Chem. Soc. XXXX, XXX, XXX−XXX

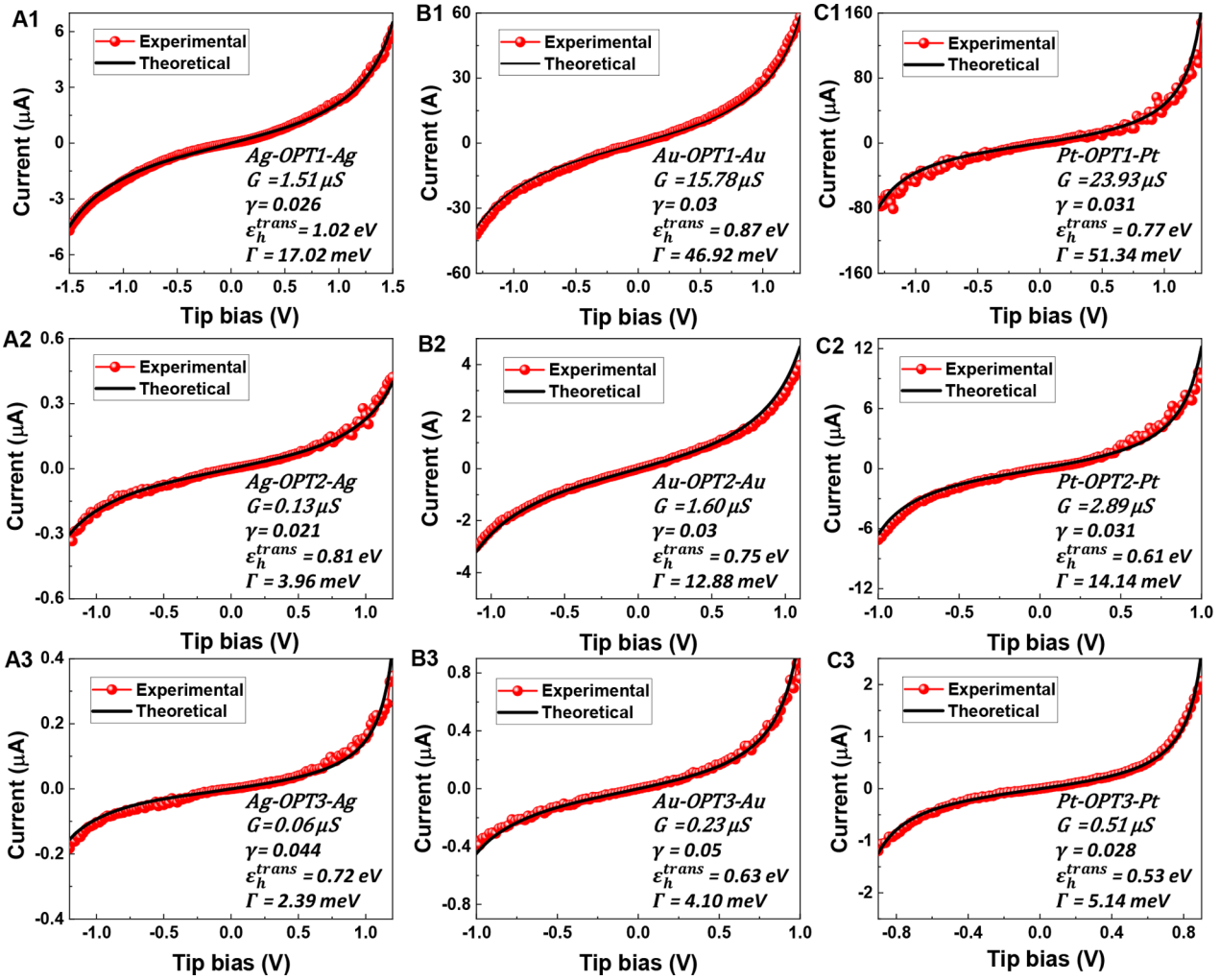

Figure 5. Experimental $I-V$ curves (red) and single-level model simulations via eq 5 (black) for (A1−3) Ag−OPTn−Ag, (B1−3) Au−OPTn−Au, and (C1−3) Pt−OPTn−Pt junctions. The three extracted parameters for each junction, low bias conductance G ($1/R$), the energy offset ε_h^{trans} and orbital shift factor γ are listed in each panel. The calculated coupling strengths Γ (calculated from G via eq 6) are also provided. Note that G is determined by the (ohmic) low bias conductance and ε_h^{trans} and γ are determined from transition voltage plots (Figure 3C) and eqs 2 and 4. Thus, none of the parameters shown are freely adjusted.

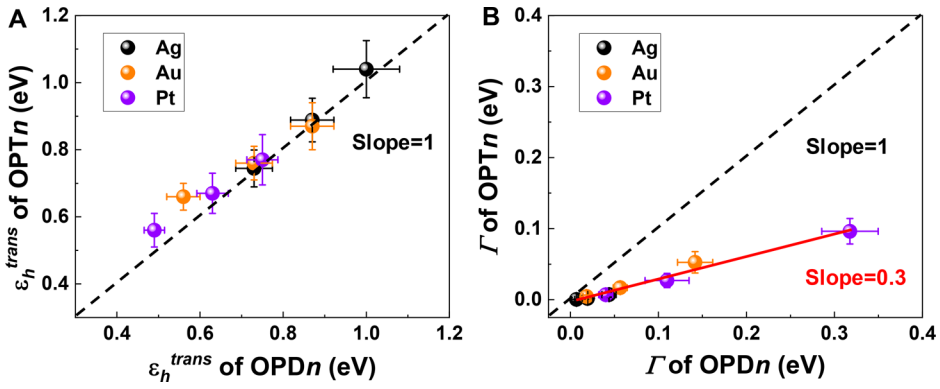

Figure 6. HOMO energy offset ε_h^{trans} (A) and coupling Γ (B) for OPTn vs OPDn with Ag, Au, and Pt contacts. ε_h^{trans} and Γ were extracted from $I-V$ characteristics using the single-level model. The dashed lines show the trends for perfect correspondence. The red line in panel B represents the linear fit.

systematically, $\Gamma_{Ag} < \Gamma_{Au} < \Gamma_{Pt}$, with an exponential falloff with increasing length n in each molecular set as well. Thus, we ascribe the strong change in junction resistance R (Figure 2) to be primarily related to the changes in Γ^2.

Simulation of $I-V$ Curves Using the Single-Level Model. An important verification of the SLM is whether it accurately predicts the measured $I-V$ behavior. Using the extracted values of ε_h^{trans}, γ, and low bias G (from which we

DOI: 10.1021/jacs.8b13370
J. Am. Chem. Soc. XXXX, XXX, XXX−XXX

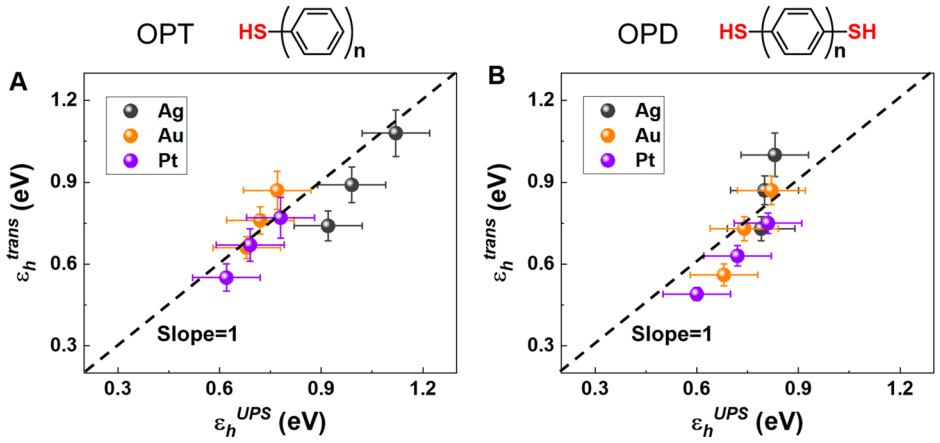

Figure 7. Correlation of ε_h^{trans} from transport measurements (and the single-level model) with ε_h^{UPS} from UPS measurements for (A) OPT*n* and (B) OPD*n* molecular junctions with Ag, Au, and Pt contacts. The dashed lines show the trends for perfect correspondence.

calculate Γ directly by eq 6), the *I*−*V* data for all junctions were simulated with eq 5. Indeed, eq 5 reproduces the individual *I*−*V* curves measured for our CP-AFM junctions extremely well, as shown in Figure 5 for individual *I*−*V* traces collected from nine Ag−OPT*n*−Ag, Au−OPT*n*−Au, and Pt−OPT*n*−Pt junctions. The fitting of symmetric OPD*n* junctions has been reported previously.[42] Importantly, *G*, ε_h^{trans}, and γ in eq 5 were not taken as adjustable parameters to achieve these fits. Rather, *G* is obtained directly from the measured low bias resistance, and ε_h and γ are calculated via eqs 2 and 4 from the measured transition voltage V_t (see Figures 3 and 4). These values were inserted into eq 5 to compute the *I*−*V* traces directly, which indeed matched the data. Of course, this is really a self-consistency check as eqs 2 and 4 derive from the SLM described by eq 5. We believe the high quality of the simulations justifies the use of the single-level model for analysis of the OPT*n* and OPD*n* molecular junctions; we provide further support for the SLM below.

Comparison of OPT*n* and OPD*n* Transport. For a given type of electrode and the same number of phenylene repeat units (*n*), the resistance of a dithiol junction (OPD*n*) is always smaller than its monothiol (OPT*n*) counterpart by 1−2 orders of magnitude (Figure 2),[42] although the OPD*n* length is larger than the OPT*n* length by the extra S-metal bond. The higher resistance of OPT*n* versus OPD*n* junctions is ascribed to the different nature of the top contact (physisorbed versus chemisorbed).[51,62−67] Figure 6A and Table 2 show that, interestingly, there is no obvious difference in the energy offset ε_h^{trans} (or tunneling barrier) induced by the different nature of the contacts; the ε_h^{trans} values of OPT*n* are remarkably close to that of OPD*n*, Table 2. Thus, differences in ε_h cannot explain the large conductance difference between OPT*n* and OPD*n* junctions. The conductance difference between dithiols and monothiols is due to Γ. As shown in Figure 6B (and listed in Table 2), the average Γ of OPD*n* are higher than OPT*n* by factors of 3−15 depending on length and metal type, which results in 1−2 orders of magnitude difference in junction resistance (eq 6, $R \propto {}^{1}/_{\Gamma^2}$). Γ is proportional to the square root of Γ_t (cf. eq 6), and Γ_t for the phenyl/tip contact is correspondingly smaller than for the thiol/tip contact. The findings here for OPT*n* versus OPD*n* are consistent with numerous examples in the literature for two-terminal tunnel junctions in that two chemical contacts lead to higher junction conductances than one chemical and one physical contact.[51,64−70]

UPS Measurements of ε_h and Implications. To obtain independent verification of the energy level alignment ε_h^{trans} determined by transport, we undertook analysis of OPT*n* and OPD*n* SAMs by UPS, which is the standard experimental method to sample occupied electronic states.[71−73] The spectra for OPT1−3 and OPD1−3 on Ag, Au, and Pt substrates, respectively are shown in Figures S4 and S5 in the Supporting Information. In these binding energy spectra, the Fermi edge is clearly evident and the HOMO onsets were determined using standard extrapolation protocols as indicated.[53,54] The resulting 18 ε_h^{UPS} values obtained by UPS for OPT1−3 and OPD1−3 are compared to the corresponding 18 ε_h^{trans} values obtained by transport (Table 2 and Figure 7). For OPT*n*, agreement between ε_h^{UPS} and ε_h^{trans} is excellent; most of the data points in Figure 7A lie, within error, on the slope = 1 trendline, i.e., ε_h^{UPS} and ε_h^{trans} are essentially the same, within error. For OPD*n*, Figure 7B, the correspondence is also reasonable, but not as good as for OPT*n*. However, we might anticipate greater deviation between ε_h^{UPS} and ε_h^{trans} for OPD*n* because the additional −SH functional group of the OPD molecules provides a terminal dipole that can affect ionization potentials in UPS. In light of the potential complexity that the terminal −SH introduces for UPS measurements on OPD*n* compared to OPT*n*, the good correlation evident in Figure 7B is gratifying.

Two important points follow here. First, the general agreement between ε_h^{UPS} and ε_h^{trans} is an important validation of the SLM for OPT*n* and OPD*n* junctions, as SLM was central to determining ε_h^{trans}. The applicability of SLM to molecular junctions has been emphasized by us many times,[42−45,47] and indeed, we have noted that for the experimentalist the ability to rapidly extract important electronic structure parameters from *I*−*V* characteristics with a simple analytical model is invaluable. Until now, however, we have not presented clear evidence that the energies obtained from the model have direct correspondence with the independently measured electronic structure of the junction. The agreement in Figure 7 is thus a critical demonstration.

Second, we note that ε_h^{UPS} and ε_h^{trans} agree in spite of the fact that the UPS measurement probes only "half the junction" (i.e., there is no second contact), and this has important implications for the mechanism of energy level alignment.

DOI: 10.1021/jacs.8b13370
J. Am. Chem. Soc. XXXX, XXX, XXX−XXX

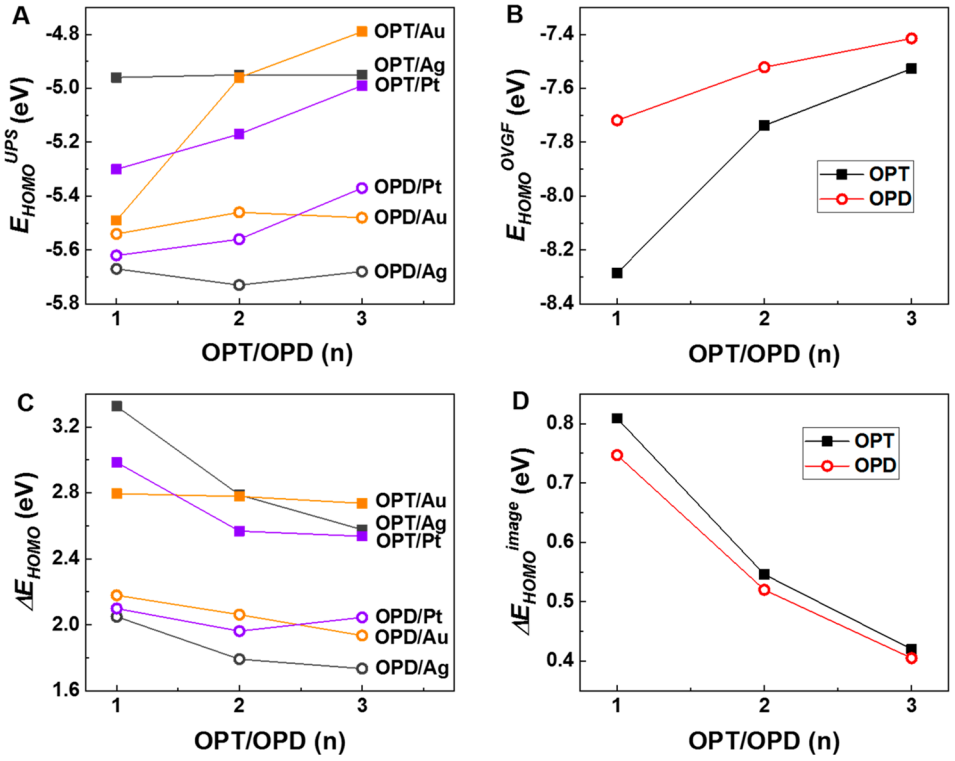

Figure 8. (A) HOMO energies relative to the vacuum level, $E^{UPS}_{HOMO} = -(\Phi_{SAM} + \varepsilon_h^{UPS})$, of OPT*n* and OPD*n* SAMs adsorbed on Ag, Au, Pt substrates obtained via UPS measurements (see also Table 2). (B) HOMO energies E^{OVGF}_{HOMO} for the isolated OPT*n* and OPD*n* molecules obtained via OVGF calculations. (C) Shift in HOMO energies $\Delta E_{HOMO} = E^{UPS}_{HOMO} - E^{OVGF}_{HOMO}$ for OPT*n* and OPD*n* SAMs relative to the isolated molecules. (D) Shift in HOMO energies expected in the case of image charge effects. For this calculation, a typical value $\varepsilon_r = 2.3$ was used for the dielectric constant of the SAMs.

Evidently, binding of an OPT or OPD molecule to a metal via a single thiol group essentially fixes ε_h; introducing a second, chemically or physically bonded metal contact has a minimal impact on ε_h. This finding implies that image charge effects, commonly invoked in discussions of energy level alignment in molecular junctions, must be reasonably small, as the effects of a second contact would be expected to be roughly additive. By "energy level alignment" we mean the upward or downward shifts of occupied or unoccupied MOs, respectively, relative to the same MOs in the isolated, gas-phase state. To emphasize our point regarding the role of image charges, we make a quantitative comparison below of the total HOMO shift measured for OPT*n* and OPD*n* on binding to a metal substrate and the predicted image charge shift due to proximity of the metal substrate.

The upward shifts of the HOMOs for OPT*n* and OPD*n* SAMs can be estimated by taking the difference between the HOMO ionization potential (IP) measured here by UPS (E^{UPS}_{HOMO}) and the gas phase IP of the isolated molecules. The experimental values of E^{UPS}_{HOMO} for OPT*n* and OPD*n* SAMS are shown in Figure 8A. Unfortunately, IPs of the isolated OPT*n* and OPTD*n* molecules are not generally known and so must be calculated. Only data for benzenethiol (OPT1) in the gas phase exist. The experimental value IP ≈ 8.3 eV of the lowest ionization energy can be trusted, as it was measured by means of a variety of methods (photoelectron spectroscopy, time-resolved dissociation, charge transfer spectroscopy, photo-ionization mass spectroscopy).[74−77] For the isolated OPT1, the outer valence Green's function (OVGF) approach using 6-311++g(d, p) basis sets as implemented in the GAUSSIAN 09 package[78] yields the value $-E^{0,OVGF}_{HOMO}$ = IE = 8.285 eV, which excellently agrees with the experimental value. In view of this agreement, we are confident that using the theoretical OVGF/6-311++g(d, p) estimates of $E^{0,OVGF}_{HOMO}$ for all of the isolated molecular species OPT*n* and OPD*n* is justified.

We note parenthetically that with the 6-311++g(d,p) basis sets the DFT approaches based on the LDA and GGA-PBE exchange correlation functionals—which belong to the class of nonhybrid exchange-correlation functionals (the only ones implemented in available packages for molecular transport (like SIESTA and ATK))—predict for the isolated OPT1 molecule values of the Kohn−Sham HOMO energy $E^{0,KS}_{HOMO}$ amounting to −6.021 and −5.416 eV, respectively. Because, in principle, DFT approaches based on hybrid exchange-correlation functionals might perform better, we computed the Kohn−Sham HOMO energy values of −6.404 eV and −6.208 eV by employing PBE0 and B3LYP, respectively, that is, two of the most recommended hybrid exchange-correlation functionals. It should be clear from above that a quantitative analysis of image charge effects based on DFT estimates of the HOMO energies cannot be trusted.

The OVGF results for E^{0}_{HOMO} of the isolated OPT*n* and OPD*n* are depicted in Figure 8B. By subtracting the complete HOMO energies of the isolated molecules (Table S2 and Figure 8B) from the HOMO energies of the molecules coupled to substrates obtained via UPS (Table 2 and Figure 8A) we estimate the shifts $\Delta E^{0}_{HOMO} = E^{UPS}_{HOMO} - E^{0}_{HOMO}$ in the HOMO energies due to the substrate, which are shown in Figure 8C. The shifts are on the order of 2−3 eV. The question is its origin: is it due predominantly to metal−molecule bonding or to image charge effects?

DOI: 10.1021/jacs.8b13370
J. Am. Chem. Soc. XXXX, XXX, XXX−XXX

Upward (downward) energy shifts of occupied (unoccupied) molecular orbitals of molecules adsorbed on electrodes with respect to their positions in isolated molecules are often assigned as image charge effects in literature,[34,79] *i.e.*, the decreases in ionization potentials (electron affinities) for orbitals in the vicinity of a metal.[80] Given the delocalized nature of the HOMOs in both OPT*n* and OPD*n* (cf. Figure S7), the popular description assuming a pointlike MO is not adequate.[79,81] For delocalized orbitals, integration over the spatial MO distribution is needed to estimate the image-driven MO shift.[82] The HOMO energy shifts obtained for OPT*n* and OPD*n* by applying this procedure explained in detail in ref 82 are presented in Figure 8D. As the image-driven shifts in Figure 8D are 15−35% of the estimated HOMO shifts in Figure 8C, the cause of the HOMO energy shifts for OPT*n* and OPD*n* SAMs on Ag, Au, and Pt can be safely said to be largely due to S−metal covalent bonding, not image charge effects. Although this conclusion may be surprising in view of the increasing popularity of assigning MO shifts in molecular electronic devices to image charges, it is fully in line with well-established wisdom.[72] Shifts due to electrostatic interactions with image charges are expected to be important for electronic states of the absorbed molecule that are localized on the adsorbate rather than shared in covalent bonds with the electrodes.[72] Clearly, the latter situation is the case for OPT*n* and OPD*n* systems anchored via thiol groups forming strong covalent S−M (M = Ag, Au, Pt) bonds.

CONCLUSION

Our combined experimental and single-level model analysis of transport for OPT*n* monothiols with Ag, Au, and Pt contacts reveals both notable similarities and differences with the previously reported results for OPD*n* dithiols.[42] Specifically, the effective tunnel barrier ε_h is the same within error for the two systems and is only weakly dependent on molecular length n and metal work function Φ, whereas in stark contrast, the molecule−electrode electronic coupling Γ is significantly higher for OPD*n* than for OPT*n* and is strongly dependent on n and Φ. Several conclusions follow from these results, namely that (1) chemically bonded (i.e., metal−S) contacts produce larger electronic couplings Γ, as has been shown in the literature,[70,83] and thus, the second (tip-SAM) contact has a large effect on Γ; (2) the second (tip-SAM) contact has only a weak effect on ε_h, meaning that ε_h is effectively set for OPT*n* and OPD*n* by the first metal−S bond; (3) the length dependence of transport characterized by the empirical attenuation factor β is largely determined by Γ, not ε_h, for both OPT*n* and OPD*n* with all three metal contacts; (4) Fermi level pinning, i.e., a weak dependence of ε_h on Φ, is germane to both OPT*n* and OPD*n*, which corresponds well with prior reports on other SAMs systems; (5) correspondingly, the Φ dependence of transport, which can be empirically characterized by the contact resistance R_c, is largely dependent on Γ, not ε_h.

Most significantly, our independent measurements of the occupied electronic states of OPT*n* and OPD*n* SAMs by UPS provide values of ε_h^{UPS} that agree remarkably well with the transport estimates ε_h^{trans} for both systems. This provides compelling support for the application of the single-level model to the analysis of OPT*n* and OPD*n* molecular junctions. The relevance of the SLM for molecular junctions has so far been based on the outstanding fits of the SLM to the $I-V$ characteristics of junctions composed of a wide range of molecules. The comparison with UPS results reported here is the first time that the extracted values of ε_h^{trans} have been shown to be in excellent agreement with electronic spectroscopy, and thus provides an important demonstration of the value of the SLM for the case of these simple molecular junctions. Our corroborating OVGF calculations have further shown that ε_h is largely set by the metal−S bonding (i.e., quantum mechanical effects) and not by classical image charge stabilization. Overall, our results provide a more complete physical picture for the electronic factors impacting tunneling in SAM-based molecular junctions and demonstrate the utility of the compact single-level model for aiding the analysis of structure-transport relationships.

ASSOCIATED CONTENT

Supporting Information

The Supporting Information is available free of charge on the ACS Publications website at DOI: 10.1021/jacs.8b13370.

Experimental and theoretical details, supplementary tables and figures (PDF)

AUTHOR INFORMATION

Corresponding Authors

*ioan.baldea@pci.uni-heidelberg.de
*frisbie@umn.edu

ORCID

Zuoti Xie: 0000-0002-1828-0122
Ioan Bâldea: 0000-0003-4860-5757
C. Daniel Frisbie: 0000-0002-4735-2228

Notes

The authors declare no competing financial interest.

ACKNOWLEDGMENTS

C.D.F. acknowledges financial support from the U.S. National Science Foundation (CHE-1708173). Parts of this work were carried out in the Characterization Facility, University of Minnesota, which receives partial support from NSF through the MRSEC program. I.B. acknowledges financial support from the Deutsche Forschungsgemeinschaft (DFG grant BA 1799/3-1), and computational support from the State of Baden-Württemberg through bwHPC and the DFG through Grant No. INST 40/467-1 FUGG.

REFERENCES

(1) Donhauser, Z. J.; Mantooth, B. A.; Kelly, K. F.; Bumm, L. A.; Monnell, J. D.; Stapleton, J. J.; Price, D. W., Jr; Rawlett, A. M.; Allara, D. L.; Tour, J. M.; Weiss, P. S. Conductance Switching in Single Molecules through Conformational Changes. *Science* **2001**, *292*, 2303−2307.

(2) Holmlin, R. E.; Haag, R.; Chabinyc, M. L.; Ismagilov, R. F.; Cohen, A. E.; Terfort, A.; Rampi, M. A.; Whitesides, G. M. Electron Transport through Thin Organic Films in Metal−insulator−metal Junctions Based on Self-Assembled Monolayers. *J. Am. Chem. Soc.* **2001**, *123*, 5075−5085.

(3) Díez-Pérez, I.; Hihath, J.; Lee, Y.; Yu, L.; Adamska, L.; Kozhushner, M. A.; Oleynik, I. I.; Tao, N. J. Rectification and Stability of a Single Molecular Diode with Controlled Orientation. *Nat. Chem.* **2009**, *1*, 635−641.

(4) McCreery, R. L.; Bergren, A. J. Progress with Molecular Electronic Junctions: Meeting Experimental Challenges in Design and Fabrication. *Adv. Mater.* **2009**, *21*, 4303−4322.

DOI: 10.1021/jacs.8b13370
J. Am. Chem. Soc. XXXX, XXX, XXX−XXX

(5) Song, H.; Kim, Y.; Jang, Y. H.; Jeong, H.; Reed, M. A.; Lee, T. Observation of Molecular Orbital Gating. *Nature* **2009**, *462*, 1039−1043.
(6) Wang, G.; Kim, T.-W.; Lee, T. Electrical Transport Characteristics through Molecular Layers. *J. Mater. Chem.* **2011**, *21*, 18117−18136.
(7) Amdursky, N.; Marchak, D.; Sepunaru, L.; Pecht, I.; Sheves, M.; Cahen, D. Electronic Transport via Proteins. *Adv. Mater.* **2014**, *26*, 7142−7161.
(8) Meng, F.; Hervault, Y.-M.; Shao, Q.; Hu, B.; Norel, L.; Rigaut, S.; Chen, X. Orthogonally Modulated Molecular Transport Junctions for Resettable Electronic Logic Gates. *Nat. Commun.* **2014**, *5*, 3023.
(9) Manrique, D. Z.; Huang, C.; Baghernejad, M.; Zhao, X.; Al-Owaedi, O. A.; Sadeghi, H.; Kaliginedi, V.; Hong, W.; Gulcur, M.; Wandlowski, T.; Bryce, M. R.; Lambert, C. J. A Quantum Circuit Rule for Interference Effects in Single-Molecule Electrical Junctions. *Nat. Commun.* **2015**, *6*, 6389.
(10) Artes, J. M.; Li, Y.; Qi, J.; Anantram, M. P.; Hihath, J. Conformational Gating of DNA Conductance. *Nat. Commun.* **2015**, *6*, 8870.
(11) Aragones, A. C.; Aravena, D.; Cerda, J. I.; Acís-Castillo, Z.; Li, H.; Real, J. A.; Sanz, F.; Hihath, J.; Ruiz, E.; Díez-Pérez, I. Large Conductance Switching in a Single-Molecule Device through Room Temperature Spin-Dependent Transport. *Nano Lett.* **2016**, *16*, 218−226.
(12) Xiang, D.; Wang, X.; Jia, C.; Lee, T.; Guo, X. Molecular-Scale Electronics : From Concept to Function. *Chem. Rev.* **2016**, *116*, 4318−4440.
(13) Nitzan, A.; Ratner, M. A. Electron Transport in Molecular Wire Junctions. *Science* **2003**, *300*, 1384−1389.
(14) Xiang, L.; Hines, T.; Palma, J. L.; Lu, X.; Mujica, V.; Ratner, M. A.; Zhou, G.; Tao, N. J. Non-Exponential Length Dependence of Conductance in Iodide-Terminated Oligothiophene Single-Molecule Tunneling Junctions. *J. Am. Chem. Soc.* **2016**, *138*, 679−687.
(15) Li, Y.; Haworth, N. L.; Xiang, L.; Ciampi, S.; Coote, M. L.; Tao, N. Mechanical Stretching-Induced Electron-Transfer Reactions and Conductance Switching in Single Molecules. *J. Am. Chem. Soc.* **2017**, *139*, 14699−14706.
(16) Guo, X.; Small, J. P.; Klare, J. E.; Wang, Y.; Purewal, M. S.; Tam, I. W.; Hong, B. H.; Caldwell, R.; Huang, L.; O'Brien, S.; Yan, J. M.; Breslow, R.; Wind, S. J.; Hone, J.; Kim, P.; Nuckolls, C. Covalently Bridging Gaps in Single-Walled Carbon Nanotubes with Conducting Molecules. *Science* **2006**, *311*, 356−359.
(17) Venkataraman, L.; Klare, J. E.; Nuckolls, C.; Hybertsen, M. S.; Steigerwald, M. L. Dependence of Single-Molecule Junction Conductance on Molecular Conformation. *Nature* **2006**, *442*, 904−907.
(18) Lindsay, S. M.; Ratner, M. A. Molecular Transport Junctions: Clearing Mists. *Adv. Mater.* **2007**, *19*, 23−31.
(19) Ho Choi, S.; Kim, B.; Frisbie, C. D. Electrical Resistance of Long Conjugated Molecular Wires. *Science* **2008**, *320*, 1482−1486.
(20) Liu, K.; Wang, X.; Wang, F. Probing Charge Transport of Ruthenium-Complex-Based Molecular Wires at the Single-Molecule Level. *ACS Nano* **2008**, *2*, 2315−2323.
(21) Bogani, L.; Wernsdorfer, W. Molecular Spintronics Using Single-Molecule Magnets. *Nat. Mater.* **2008**, *7*, 179−186.
(22) Nijhuis, C. A.; Reus, W. F.; Whitesides, G. M. Molecular Rectification in Metal-SAM-Metal Oxide-Metal Junctions. *J. Am. Chem. Soc.* **2009**, *131*, 17814−17827.
(23) Mishchenko, A.; Vonlanthen, D.; Meded, V.; Bürkle, M.; Li, C.; Pobelov, I. V.; Bagrets, A.; Viljas, J. K.; Pauly, F.; Evers, F.; Mayor, M.; Wandlowski, T. Influence of Conformation on Conductance of Biphenyl-Dithiol Single-Molecule Contacts. *Nano Lett.* **2010**, *10*, 156−163.
(24) Zhen, S.; Mao, J. C.; Chen, L.; Ding, S.; Luo, W.; Zhou, X. S.; Qin, A.; Zhao, Z.; Tang, B. Z. Remarkable Multichannel Conductance of Novel Single-Molecule Wires Built on Through-Space Conjugated Hexaphenylbenzene. *Nano Lett.* **2018**, *18*, 4200−4205.
(25) Su, T. A.; Neupane, M.; Steigerwald, M. L.; Venkataraman, L.; Nuckolls, C. Chemical Principles of Single-Molecule Electronics. *Nat. Rev. Mater.* **2016**, *1*, 16002.
(26) Yelin, T.; Korytar, R.; Sukenik, N.; Vardimon, R.; Kumar, B.; Nuckolls, C.; Evers, F.; Tal, O. Conductance Saturation in a Series of Highly Transmitting Molecular Junctions. *Nat. Mater.* **2016**, *15*, 444−449.
(27) Garner, M. H.; Li, H.; Chen, Y.; Su, T. A.; Shangguan, Z.; Paley, D. W.; Liu, T.; Ng, F.; Li, H.; Xiao, S.; Nuckolls, C.; Venkataraman, L.; Solomon, G. C. Comprehensive Suppression of Single-Molecule Conductance Using Destructive σ-Interference. *Nature* **2018**, *558*, 415−419.
(28) Kim, T.; Darancet, P.; Widawsky, J. R.; Kotiuga, M.; Quek, S. Y.; Neaton, J. B.; Venkataraman, L. Determination of Energy Level Alignment and Coupling Strength in 4,4′ -Bipyridine Single-Molecule Junctions. *Nano Lett.* **2014**, *14*, 794−798.
(29) Malen, J. A.; Doak, P.; Baheti, K.; Tilley, T. D.; Segalman, R. A.; Majumdar, A. Identifying the Length Dependence of Orbital Alignment and Contact Coupling in Molecular Heterojunctions. *Nano Lett.* **2009**, *9*, 1164−1169.
(30) Ko, C.-H.; Huang, M.-J.; Fu, M.-D.; Chen, C.-H. Superior Contact for Single-Molecule Conductance: Electronic Coupling of Thiolate and Isothiocyanate on Pt, Pd, and Au. *J. Am. Chem. Soc.* **2010**, *132*, 756−764.
(31) Kaliginedi, V.; Moreno-García, P.; Valkenier, H.; Hong, W.; García-Suárez, V. M.; Buiter, P.; Otten, J. L. H.; Hummelen, J. C.; Lambert, C. J.; Wandlowski, T. Correlations between Molecular Structure and Single-Junction Conductance: A Case Study with Oligo(Phenylene-Ethynylene)-Type Wires. *J. Am. Chem. Soc.* **2012**, *134*, 5262−5275.
(32) Van Dyck, C.; Ratner, M. A. Molecular Rectifiers: A New Design Based on Asymmetric Anchoring Moieties. *Nano Lett.* **2015**, *15*, 1577−1584.
(33) Diez-Cabanes, V.; Gonzalez, S. R.; Osella, S.; Cornil, D.; Van Dyck, C.; Cornil, J. Energy Level Alignment at Interfaces between Au (111) and Thiolated Oligophenylenes of Increasing Chain Size : Theoretical Evidence of Pinning Effects. *Adv. Thoery Simulations* **2018**, *1*, 1700020.
(34) Quek, S. Y.; Choi, H. J.; Louie, S. G.; Neaton, J. B. Length Dependence of Conductance in Aromatic Single-Molecule Junctions. *Nano Lett.* **2009**, *9*, 3949−3953.
(35) Zhang, N.; Lo, W. Y.; Cai, Z.; Li, L.; Yu, L. Molecular Rectification Tuned by Through-Space Gating Effect. *Nano Lett.* **2017**, *17*, 308−312.
(36) Kim, Y.; Jeong, W.; Kim, K.; Lee, W.; Reddy, P. Electrostatic Control of Thermoelectricity in Molecular Junctions. *Nat. Nanotechnol.* **2014**, *9*, 881−885.
(37) Xiang, L.; Palma, J. L.; Li, Y.; Mujica, V.; Ratner, M. A.; Tao, N. Gate-Controlled Conductance Switching in DNA. *Nat. Commun.* **2017**, *8*, 14471.
(38) Yuan, L.; Wang, L.; Garrigues, A. R.; Jiang, L.; Annadata, H. V.; Anguera Antonana, M.; Barco, E.; Nijhuis, C. A. Transition from Direct to Inverted Charge Transport Marcus Regions in Molecular Junctions via Molecular Orbital Gating. *Nat. Nanotechnol.* **2018**, *13*, 322−329.
(39) Capozzi, B.; Chen, Q.; Darancet, P.; Kotiuga, M.; Buzzeo, M.; Neaton, J. B.; Nuckolls, C.; Venkataraman, L. Tunable Charge Transport in Single-Molecule Junctions via Electrolytic Gating. *Nano Lett.* **2014**, *14*, 1400−1404.
(40) Kayser, B.; Fereiro, J. A.; Guo, C.; Cohen, S. R.; Sheves, M.; Pecht, I.; Cahen, D. Transistor Configuration Yields Energy Level Control in Protein-Based Junctions. *Nanoscale* **2018**, *10*, 21712−21720.
(41) Bâldea, I. Ambipolar Transition Voltage Spectroscopy: Analytical Results and Experimental Agreement. *Phys. Rev. B: Condens. Matter Mater. Phys.* **2012**, *85*, 035442.
(42) Xie, Z.; Bâldea, I.; Smith, C. E.; Wu, Y.; Frisbie, C. D. Experimental and Theoretical Analysis of Nanotransport in

DOI: 10.1021/jacs.8b13370
J. Am. Chem. Soc. XXXX, XXX, XXX−XXX

Oligophenylene Dithiol Junctions as a Function of Molecular Length and Contact Work Function. *ACS Nano* **2015**, *9*, 8022−8036.
(43) Smith, C. E.; Xie, Z.; Baldea, I.; Frisbie, C. D. Work Function and Temperature Dependence of Electron Tunneling through an N-Type Perylene Diimide Molecular Junction with Isocyanide Surface Linkers. *Nanoscale* **2018**, *10*, 964.
(44) Xie, Z.; Bâldea, I.; Frisbie, C. D. Why One Can Expect Large Rectification in Molecular Junctions Based on Alkane Monothiols and Why Rectification Is So Modest. *Chem. Sci.* **2018**, *9*, 4456−4467.
(45) Xie, Z.; Bâldea, I.; Oram, S.; Smith, C. E.; Frisbie, C. D. Effect of Heteroatom Substitution on Transport in Alkane Dithiol-Based Molecular Tunnel Junctions: Evidence for Universal Behavior. *ACS Nano* **2017**, *11*, 569−578.
(46) Xie, Z.; Bâldea, I.; Haugstad, G.; Frisbie, C. D. Mechanical Deformation Distinguishes Tunneling Pathways in Molecular Junctions. *J. Am. Chem. Soc.* **2019**, *141*, 497−504.
(47) Rodriguez-Gonzalez, S.; Xie, Z.; Galangau, O.; Selvanathan, P.; Norel, L.; Van Dyck, C.; Costuas, K.; Frisbie, C. D.; Rigaut, S.; Cornil, J. HOMO Level Pinning in Molecular Junctions: Joint Theoretical and Experimental Evidence. *J. Phys. Chem. Lett.* **2018**, *9*, 2394−2403.
(48) Bâldea, I.; Xie, Z.; Frisbie, C. D. Uncovering a Law of Corresponding States for Electron Tunneling in Molecular Junctions. *Nanoscale* **2015**, *7*, 10465−10471.
(49) Kim, B.; Beebe, J. M.; Jun, Y.; Zhu, X.-Y.; Frisbie, C. D. Correlation between HOMO Alignment and Contact Resistance in Molecular Junctions: Aromatic Thiols versus Aromatic Isocyanides. *J. Am. Chem. Soc.* **2006**, *128*, 4970−4971.
(50) Salomon, A.; Boecking, T.; Seitz, O.; Markus, T.; Amy, F.; Chan, C.; Zhao, W.; Cahen, D.; Kahn, A. What Is the Barrier for Tunneling Through Alkyl Monolayers? Results from n- and p-Si−Alkyl/Hg Junctions. *Adv. Mater.* **2007**, *19*, 445−450.
(51) Kim, B.; Choi, S. H.; Zhu, X.-Y.; Frisbie, C. D. Molecular Tunnel Junctions Based on π-Conjugated Oligoacene Thiols and Dithiols between Ag, Au, and Pt Contacts: Effect of Surface Linking Group and Metal Work Function. *J. Am. Chem. Soc.* **2011**, *133*, 19864−19877.
(52) Sayed, S. Y.; Fereiro, J. A.; Yan, H.; McCreery, R. L.; Bergren, A. J. Charge Transport in Molecular Electronic Junctions: Compression of the Molecular Tunnel Barrier in the Strong Coupling Regime. *Proc. Natl. Acad. Sci. U. S. A.* **2012**, *109*, 11498−11503.
(53) Yaffe, O.; Qi, Y.; Scheres, L.; Puniredd, S. R.; Segev, L.; Ely, T.; Haick, H.; Zuilhof, H.; Vilan, A.; Kronik, L.; Kahn, A.; Cahen, D. Charge Transport across Metal/Molecular (Alkyl) Monolayer-Si Junctions Is Dominated by the LUMO Level. *Phys. Rev. B: Condens. Matter Mater. Phys.* **2012**, *85*, 045433.
(54) Souto, M.; Díez-Cabanes, V.; Yuan, L.; Kyvik, A. R.; Ratera, I.; Nijhuis, C. A.; Cornil, J.; Veciana, J. Influence of the Donor Unit on the Rectification Ratio in Tunnel Junctions Based on Donor-Acceptor SAMs Using PTM Units as Acceptors. *Phys. Chem. Chem. Phys.* **2018**, *20*, 25638−25647.
(55) Xie, Z.; Bâldea, I.; Demissie, A. T.; Smith, C. E.; Wu, Y.; Haugstad, G.; Frisbie, C. D. Exceptionally Small Statistical Variations in the Transport Properties of Metal−Molecule−Metal Junctions Composed of 80 Oligophenylene Dithiol Molecules. *J. Am. Chem. Soc.* **2017**, *139*, 5696−5699.
(56) Demissie, A. T.; Haugstad, G.; Frisbie, C. D. Quantitative Surface Coverage Measurements of Self-Assembled Monolayers by Nuclear Reaction Analysis of Carbon-12. *J. Phys. Chem. Lett.* **2016**, *7*, 3477−3481.
(57) Engelkes, V. B.; Beebe, J. M.; Frisbie, C. D. Length-Dependent Transport in Molecular Junctions Based on SAMs of Alkanethiols and Alkanedithiols: Effect of Metal Work Function and Applied Bias on Tunneling Efficiency and Contact Resistance. *J. Am. Chem. Soc.* **2004**, *126*, 14287−14296.
(58) Kim, T.; Vázquez, H.; Hybertsen, M. S.; Venkataraman, L. Conductance of Molecular Junctions Formed with Silver Electrodes. *Nano Lett.* **2013**, *13*, 3358−3364.
(59) Bâldea, I. Important Issues Facing Model-Based Approaches to Tunneling Transport in Molecular Junctions. *Phys. Chem. Chem. Phys.* **2015**, *17*, 20217−20230.
(60) Beebe, J. M.; Kim, B.; Gadzuk, J. W.; Frisbie, C. D.; Kushmerick, J. G. Transition from Direct Tunneling to Field Emission in Metal-Molecule-Metal Junctions. *Phys. Rev. Lett.* **2006**, *97*, 026801.
(61) Zahid, F.; Paulsson, M.; Datta, S. Electrical Conduction through Molecules In *Advanced Semiconductors and Organic Nano-Techniques*; Morkoc, H., Ed.; Academic Press: New York, 2003; Vol. 3.
(62) Heimel, G.; Romaner, L.; Brédas, J.-L.; Zojer, E. Interface Energetics and Level Alignment at Covalent Metal-Molecule Junctions: π-Conjugated Thiols on Gold. *Phys. Rev. Lett.* **2006**, *96*, 196806.
(63) Heimel, G.; Romaner, L.; Zojer, E.; Brédas, J.-L. Toward Control of the Metal-Organic Interfacial Electronic Structure in Molecular Electronics: A First-Principles Study on Self-Assembled Monolayers of π-Conjugated Molecules on Noble Metals. *Nano Lett.* **2007**, *7*, 932−940.
(64) Wang, G.; Kim, T.; Lee, H.; Lee, T. Influence of Metal-Molecule Contacts on Decay Coefficients and Specific Contact Resistances in Molecular Junctions. *Phys. Rev. B: Condens. Matter Mater. Phys.* **2007**, *76*, 205320.
(65) Wang, G.; Kim, T.; Jang, Y. H.; Lee, T. Effects of Metal - Molecule Contact and Molecular Structure on Molecular Electronic Conduction in Nonresonant Tunneling Regime : Alkyl versus Conjugated Molecules. *J. Phys. Chem. C* **2008**, *112*, 13010−13016.
(66) Akkerman, H. B.; de Boer, B. Electrical Conduction through Single Molecules and Self-Assembled Monolayers. *J. Phys.: Condens. Matter* **2008**, *20*, 013001.
(67) Kim, T. W.; Wang, G.; Lee, H.; Lee, T. Statistical Analysis of Electronic Properties of Alkanethiols in Metal-Molecule-Metal Junctions. *Nanotechnology* **2007**, *18*, 315204.
(68) Salomon, A.; Cahen, D.; Lindsay, S.; Tomfohr, J.; Engelkes, V. B.; Frisbie, C. D. Comparison of Electronic Transport Measurements on Organic Molecules. *Adv. Mater.* **2003**, *15*, 1881−1890.
(69) Kushmerick, J. G. Metal-Molecule Contacts. *Mater. Today* **2005**, *8*, 26−30.
(70) Tan, A.; Balachandran, J.; Sadat, S.; Gavini, V.; Dunietz, B. D.; Jang, S. Y.; Reddy, P. Effect of Length and Contact Chemistry on the Electronic Structure and Thermoelectric Properties of Molecular Junctions. *J. Am. Chem. Soc.* **2011**, *133*, 8838−8841.
(71) Alloway, D. M.; Hofmann, M.; Smith, D. L.; Gruhn, N. E.; Graham, A. L.; Colorado, R.; Wysocki, V. H.; Lee, T. R.; Lee, P. A.; Armstrong, N. R. Interface Dipoles Arising from Self-Assembled Monolayers on Gold : UV - Photoemission Studies of Alkanethiols and Partially Fluorinated Alkanethiols. *J. Phys. Chem. B* **2003**, *107*, 11690−11699.
(72) Braun, S.; Salaneck, W. R.; Fahlman, M. Energy-Level Alignment at Organic/Metal and Organic/Organic Interfaces. *Adv. Mater.* **2009**, *21*, 1450−1472.
(73) Cahen, D.; Kahn, A. Electron Energetics at Surfaces and Interfaces: Concepts and Experiments. *Adv. Mater.* **2003**, *15*, 271−277.
(74) Aloisi, G. G.; Santini, S.; Sorriso, S. Molecular Complexes of Substituted Diphenyl Sulphides with π Acceptors. Charge Transfer Spectra and Ionization Potentials of the Donors. *J. Chem. Soc., Faraday Trans. 1* **1974**, *70*, 1908−1913.
(75) Faulk, J. D.; Dunbar, R. C.; Lifshitz, C. Slow Dissociations of Thiophenol Molecular Ion. Study by TRPD and TPIMS. *J. Am. Chem. Soc.* **1990**, *112*, 7893−7899.
(76) Carnovale, F.; Kibel, M. H.; Nyberg, G. L.; Peel, J. B. Photoelectron Spectroscopic Assignment of the P-States of Benzenethiol. *J. Electron Spectrosc. Relat. Phenom.* **1982**, *25*, 171−179.
(77) Ashby, M. T.; Enemark, J. H.; Lichtenberger, D. L. Destabilizing Dπ-Pπ Orbital Interactions and the Alkylation Reactions of Iron(II)-Thiolate Complexes. *Inorg. Chem.* **1988**, *27*, 191−197.

DOI: 10.1021/jacs.8b13370
J. Am. Chem. Soc. XXXX, XXX, XXX−XXX

(78) Frisch, M. J.; Trucks, G. W.; Schlegel, H. B.; Scuseria, G. E.; Robb, M. A.; Cheeseman, J. R.; Scalmani, G.; Barone, V.; Mennucci, B.; Petersson, G. A.; Nakatsuji, H.; Caricato, M.; Li, X.; Hratchian, H. P.; Izmaylov, A. F.; Bloino, J.; Zheng, G.; Sonnenberg, J. L.; Hada, M.; Ehara, M.; Toyota, K.; Fukuda, R.; Hasegawa, J.; Ishida, M.; Nakajima, T.; Honda, Y.; Kitao, O.; Nakai, H.; Vreven, T.; Montgomery, J. A., Jr; Peralta, J. E.; Ogliaro, F.; Bearpark, M.; Heyd, J. J.; Brothers, E.; Kudin, K. N.; Staroverov, V. N.; Keith, T.; Kobayashi, R.; Normand, J.; Raghavachari, K.; Rendell, A.; Burant, J. C.; Iyengar, S. S.; Tomasi, J.; Cossi, M.; Rega, N.; Millam, J. M.; Klene, M.; Knox, J. E.; Cross, J. B.; Bakken, V.; Adamo, C.; Jaramillo, J.; Gomperts, R.; Stratmann, R. E.; Yazyev, O.; Austin, A. J.; Cammi, R.; Pomelli, C.; Ochterski, J. W.; Martin, R. L.; Morokuma, K.; Zakrzewski, V. G.; Voth, G. A.; Salvador, P.; Dannenberg, J. J.; Dapprich, S.; Daniels, A. D.; Farkas, O.; Foresman, J. B.; Ortiz, J. V.; Cioslowski, J.; Fox, D. J. *Gaussian 09*, Revision B.01; Gaussian, Inc., Wallingford, CT, 2010.

(79) Neaton, J. B.; Hybertsen, M. S.; Louie, S. G. Renormalization of Molecular Electronic Levels at Metal-Molecule Interfaces. *Phys. Rev. Lett.* **2006**, *97*, 216405.

(80) Desjonqueres, M.-C.; Spanjaard, D. *Concepts in Surface Science*, 2nd ed.; Springer Verlag: Berlin, 1996.

(81) Widawsky, J. R.; Darancet, P.; Neaton, J. B.; Venkataraman, L. Simultaneous Determination of Conductance and Thermopower of Single Molecule Junctions. *Nano Lett.* **2012**, *12*, 354−358.

(82) Bâldea, I. Transition Voltage Spectroscopy Reveals Significant Solvent Effects on Molecular Transport and Settles an Important Issue in Bipyridine-Based Junctions. *Nanoscale* **2013**, *5*, 9222−9230.

(83) Vondrak, T.; Cramer, C. J.; Zhu, X.-Y. The Nature of Electronic Contact in Self-Assembled Monolayers for Molecular Electronics: Evidence for Strong Coupling. *J. Phys. Chem. B* **1999**, *103*, 8915−8919.

DOI: 10.1021/jacs.8b13370
J. Am. Chem. Soc. XXXX, XXX, XXX−XXX